2022 IEEE 23rd International Symposium on a World of Wireless, Mobile and Multimedia Networks (WoWMoM) | 978-1-6654-0876-9/22/$31.00 ©2022 IEEE | DOI: 10.1109/WoWMoM54355.2022.00071

Joint Terahertz Communication and Atmospheric Sensing in Low Earth Orbit Satellite Networks: Physical Layer Design

Sergi Aliaga, Ali J. Alqaraghuli, Josep M. Jornet

Department of Electrical and Computer Engineering
Institute for the Wireless Internet of Things
Northeastern University, Boston, MA, USA
E-mail: {aliaga.s, alqaraghuli.a, jmjornet}@northeastern.edu

***Abstract*—As the interest in the Terahertz (0.1-1THz) band grows with the technological advancements that enable communication at higher data rates, the existing use for THz-based sensing systems motivate exploration of Joint Communication and Sensing systems (JCS). Such systems can be used for the next generation of satellite constellations for the purposes of internet-backhauling, while performing scientific functions such as studying atmospheric gases. The fact that the hardware employed for both applications is highly similar, if not identical, opens the possibility of designing a new waveform that can jointly communicate and sense at the same time. In this paper, we explore Differential Absorption Radars (DAR), traditionally used for weather sensing, as a potential candidate to be operated in combination with a Chirp Spread Spectrum (CSS) modulation. We present a scenario with a satellite at Low Earth Orbit (LEO) where the CSS modulation could outperform traditional PSK modulations while making it possible to retrieve water vapor density profiles of the atmosphere with DAR. Performance of both communication and remote sensing applications are studied through simulation.**

***Index Terms*—THz Communications, Satellite Communications, Remote Sensing, Differential Absoprtion Radar, Chirp Spread Spectrum**

I. Introduction

Space-based internet is envisioned to be a key technology for the 6th generation (6G) of wireless communications [1]. This has motivated private companies, such as SpaceX, to launch massive satellite constellations in the aims of providing world-wide space-based internet [2]. Although the data rates offered by the current satellite operators utilizing Ku and Ka bands are still far from terrestrial wireless system capabilities, advances in technologies operating at Terahertz (THz) frequencies could enable higher data rates by utilizing the larger available bandwidth [3].

That being said, a recent concern for Non-Terrestrial Networks (NTN) utilizing a large number of satellites has been voiced by the scientific community, as private companies are able to capture a large LEO real estate in contrast to science-based satellites which operate under significantly lower budgets. Such concern have been voiced in especially against the launches of SpaceX Starlink in regards to its impact on ground-based astronomical observations [4].

In our vision, one way to maintain pushing 6G NTN innovation forward while also providing scientific value is to deploy Joint Communication and Sensing (JCS) satellite systems. This way, the same hardware front-ends can be used to communicate at high data rates as well as to gather scientific data, and such switching can be performed either autonomously or at the operator level. In this scenario, the THz band is then considered an ideal technology to deploy joint communication and sensing capabilities, given the high bandwidth available for communication as well as the existing use of THz-based radar and spectroscopy utilized in scientific missions [5]. The case for THz JCS becomes stronger given the ongoing development of THz front-ends that have been designed, built, tested, and flown on various scientific missions, which can be used as a starting point to carry this research.

II. Related Works

State of the art THz communication platforms, such as the TeraNova platform at Northeastern University [6], utilizes custom made front-ends that leverage NASA Jet Propulsion Laboratory (JPL)'s patented multiplier technology based on on-chip power combining [7]. These front-ends were originally created for remote sensing and are allowing the development of the first Vapor In-cloud Profiling Radar (VIPR) [8], capable of measuring in-cloud water vapor concentration utilizing a Differential Absorption Radar (DAR) principle, also known as the RF analog of the Differential Absorption LIDAR (DIAL), reviewed in [9]. Since record breaking power levels in the 170-190GHz were first achieved in [10], JPL has shown efforts towards developing DAR as a unique complementary technology to existing remote sensing devices. In [11], the use of DAR in the 173-193GHz band is first proposed, focusing on the strong water absorption line located at 183GHz. [12]–[14] are the first attempts and early development of DAR in that particular band and [15] shows the first experimental measurements of VIPR from the ground. Very recently, the first airborne measurements of VIPR are presented in [16]. Authors of this last work highlight that due to the high

This work was supported in part by the US National Science Foundation Grant CNS-2011411 and "La Caixa" Fellowship.

978-1-6654-0876-9/22/$31.00 ©2022 IEEE
DOI 10.1109/WoWMoM54355.2022.00071

absorption in the lower troposphere, DAR would have a higher range if operated from airborne or space platforms rather than ground operation. For this reason, authors in [17] present the simulation of DAR performed from a space-borne platform, concretely, a LEO satellite at 400 km of altitude.

With JCS in mind, the principles of operation of DAR, described in Sec. III-A, make it a unique radar technique to be combined with a modulation for the transmission of information. In particular, DAR operation is based on Frequency Modulated Continuous Wave (FMCW) radar because of its larger duty cycles and extremely high range resolution, compared to a pulsated system [18]. FMCW radars leverage the use of chirp signals to measure properties of a certain target. For this reason a FMCW DAR could be combined with modulations that use chirp signals too, that is, Chirp Spread Spectrum (CSS) modulations. The use of CSS modulations for the transmission of information has been studied for many years [19], [20] and has aroused attention for a long time due to its energy efficient properties [21], with LoRa being the gold standard for Low Power Wide Area Networks (LPWANs) [22]. Moreover, it has recently been shown that transmission across the water vapor absorption peaks in the THz band was possible thanks again to the use of CSS modulations [23].

In this paper, we explore the feasibility of a JCS system in the THz band utilizing the methods and technologies from state of the art and previous research carried out by the authors. Given the similarities in hardware and signal processing of DAR operated in FMCW mode and CSS, we identify an opportunity to design a waveform that jointly transmits information to an external receiver and returns, in the form of backscattered echoes, the measurements required to perform DAR. We extensively justify the use of CSS as a suitable modulation scheme to perform JCS duties, highlighting tradeoffs with comparison to traditional modulation schemes. Finally, we numerically evaluate the performance of the proposed solution and show how it can be deployed in a realistic spaceborne scenario.

The rest of the paper is structured as follows: In Sec. III, we give a high-level description of the operational principles of DAR and FMWC radars. In Sec. IV, we present the technical details of Chirp Spread Spectrum at a high level. In Sec. V, a new waveform capable of communicating and sensing at the same time is presented. In addition, a test case scenario where this new waveform performs better than traditional modulations is introduced. In Sec. VI, the performance of the presented system both at the communications receiver and at the bi-static radar receiver is presented. Finally, conclusions and future work are presented in Sec. VII.

III. Atmospheric remote sensing

As highlighted in [11], Doppler and spectroscopic radars at W (75-110 GHz) and G (110-300 GHz) bands are being developed to measure properties of different targets. Of special interest is the DAR technique used to retrieve humidity profiles inside the upper-tropospheric clouds. DAR is operated in a FMCW mode for increased sensitivity relative to a pulsated system, because the transmitter is always on. In addition, measurements required as input to the profile retrieval algorithm only depend on the echo's amplitude, i.e., Doppler measurements are not used. This is especially appealing for a joint communication and sensing system, since information bits could be encoded in the phase of the transmitted pulses without affecting the sensing capabilities of DAR. In this section we provide a high-level description of the principles of operation of DAR and FMCW Radar and outline the opportunities for the implementation of a communication system on top of it.

A. Differential Absorption Radar

The DAR profile retrieval algorithm is explained in detail in [17]. It begins with the reflectively measurements $Z_{obs}(r,f)$ derived from the received power echoes $P_e(r,f)$ through the standard weather radar equation detailed in [24]:

$$P_e(r,f) = \frac{Z(r,f)e^{-2\tau(r,f)}}{C(f)r^2} = \frac{Z_{obs}(r,f)}{C(f)r^2}, \quad (1)$$

where $C(f)$ is a radar calibration coefficient that includes all the radar parameters related to hardware and frequency dependent constants. The calibration of this coefficient is described in [8]. $Z(r,f)$ and $Z_{obs}(r,f)$ are the unattenuated and observed reflectivity factors, and $\tau(r,f)$ is the one-way optical depth. Solving for $Z_{obs}(r,f)$:

$$Z_{obs}(r,f) = P_e(r,f)C(f)r^2 \quad (2)$$

The observed reflectivity measurements can then be used to compute the observed extinction coefficient $\beta_{obs}(r,f)$ between two ranges r_1 and $r_2 = r_1 + N_b\Delta r$ as follows:

$$\beta_{obs}(r,f) = \frac{1}{2N_b\Delta r} \ln\left(\frac{Z_{obs}(r_1,f)}{Z_{obs}(r_2,f)}\right), \quad (3)$$

where $r = (r_1+r_2)/2$, Δr is the range resolution of the radar and N_b is the number of range bins considered. The relation between Δr and the radar parameters is explained in the next subsection. For small range increments $N_b\Delta r$, and assuming negligible multiple scattering, the following fitting function for $\beta_{obs}(r,f)$ is presented in [8], [17]:

$$\hat{\beta}_{obs}(r,f_i) = a_1 + a_2(f_i - f_0) + a_3 k_v(r,f_i) + \beta_{g,d}(r,f_i), \quad (4)$$

where it is assumed that measurements are made at the discrete set of frequencies $\{f_i\}$, $k_v(r,f)$ is the water vapor absorption cross section per unit mass and $\beta_{g,d}(r,f)$ is the absorption coefficient for dry air. The main purpose of DAR is to obtain the set of coefficients $\{a_i\}$ by fitting (4) to the values obtained by observation in (3) with a least-square fit. The fitted coefficients are then related to the following physical quantities in [17] as follows:

$$\begin{aligned} a_1 &\leftrightarrow \alpha(r,f_0) + \beta_h(r,f_0) \\ a_2 &\leftrightarrow \frac{\partial}{\partial f}(\alpha(r,f) + \beta_h(r,f))|_{f=f_0}, \\ a_3 &\leftrightarrow \rho_v(r) \end{aligned} \quad (5)$$

where $\alpha(r,f) = (2N_b\Delta r)^{-1}\ln[Z(r_1,f)/Z(r_2,f)]$, $\beta_h(r,f)$ is the hydrometeor extinction coefficient and $\rho_v(r)$ is the water vapor density at range r. Since three parameters are being fitted, a minimum of three transmission frequencies are required. A two-frequency approach can also be implemented, with some assumptions, but this results into biases in the retrieved profiles, as shown in [17].

We outline that to obtain the fitting parameter a_3, which is directly related to the water vapor profile along the radar range, there is no need to use Doppler measurements of the echoes received and therefore there exists the possibility to encode information bits in the phase of the signal without affecting the DAR procedure to retrieve the humidity profiles.

B. Frequency Modulated Continuous Wave Radar

Due to the low transmitted power available in its operational band (200mW in the 173-193GHz band), DAR is operated in Frequency-Modulated Continous-Wave (FMCW) mode instead of pulsated mode. FMCW radar offers increased sensitivity and higher duty cycle compared to a pulsated system because the transmitter is always on. This continuous transmission is even more appealing when considering the possibility of a communications system with the same waveform, since continuous transmission of information would be possible and no dead times waiting for echoes will be needed, as opposed to the pulsated mode.

FMCW radar uses linear chirp signals to estimate the range of back-scattering objects, or particles in the case of weather radar. As its name indicates, linear chirp signals consist of a sinusoidal wave with linearly changing frequency. Figure 1 shows a frequency-time plot of a chirp signal, outlining its main characteristic parameters.

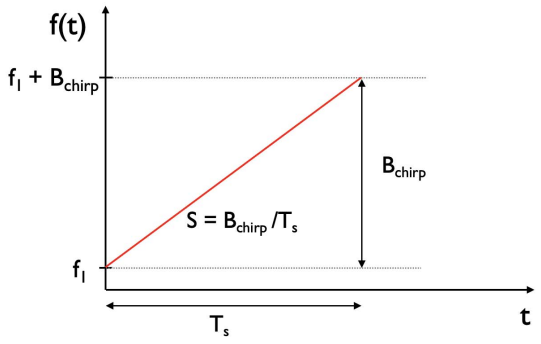

Fig. 1: Frequency-time plot of a linear chirp.

From the figure, B_{chirp} and T_s are the chirp bandwidth and period, respectively and S is the slope of the chirp. The range resolution Δr of the radar, or the minimum distance at which two object can be identified separately, can be computed as $\Delta r = c/2B_{chirp}$, where c is the speed of light. As explained before, a minimum of three transmission frequencies are required to retrieve the water vapor profiles, so a train of chirp pulses are transmitted at each different frequencies periodically to obtain the required measurements. Moreover, as highlighted in [14], triangle-wave frequency chirps are used, instead of sawtooth-wave chirps, because they provide a nearly continuous estimation of the noise floor when alternating between chirp directions. Figure 2 depicts schematically the frequency-time plot of the resulting radar with three transmission frequencies.

Both DAR and DIAL are based on the principle of transmitting at a high absorption frequency of the substance of interest and at one or more other transmission frequencies where the absorption is lower. The best way to obtain this absorption difference between the transmitted tones without requiring a large bandwidth is by transmitting close to an absorption peak. For water vapor, an absorption peak is located at 183GHZ. However, the 174.8-191.8GHz band is reserved for passive satellites sounding and transmission in those bands is not allowed [25]. For this reason, as in [17], the highest frequency of transmission considered is $f_3 = 174.8\ GHz$.

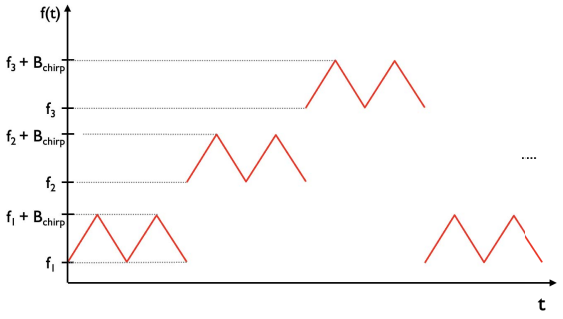

Fig. 2: FMCW radar operating at three different frequencies to obtain the measurements required for DAR

IV. Opportunity for Communications: Chirp Spread Spectrum

As mentioned, the operation of DAR only requires the observed backscattered power, or reflectivity, at different frequencies from a volume of scatterers to measure its concentration. This means that no Doppler measurements are required for that particular measure. Moreover, the operation of DAR in FMCW mode implies the use of chirp signals with little to none dead time (only a small delay when switching between frequencies). This brings an opportunity to leverage plenty of available knowledge on Chirp Spread Spectrum (CSS) modulations, which are well-known by its resilience in front of high absorption and frequency fading channels due to its larger integration times, which result in higher $\frac{E_b}{N_0}$ for a fixed SNR.

There are many different CSS modulations studied in the literature, but the fact that the amplitude and direction of the chirps is already fixed by the radar requirements, the only resource available to encode information is the signal phase.

Therefore, only Chirp Spread M-ary Phase Shift Keying (CS-MPSK) modulations will be considered. In such modulations, the set of symbols $\{s_m(t)\}$ is represented by:

$$s_m(t) = \sqrt{\frac{2}{T_s}} cos(2\pi f_0 t - \ \pi S t^2 + \ \phi_m), \quad 0 \ \leq t \ \leq T_s \quad \text{and} \quad 0 \leq m < M \tag{6}$$

where the chirp period T_s is equivalent to the symbol period, f_0 is the initial frequency and the $|S| = B_{chirp}/T_s$ is the chirp slope. The initial frequency and the sign of S will determine the direction of the chirp, which in this case is already determined by the radar mode of operation. The term ϕ_m encodes the transmitted symbol, and for an M-ary CS-MPSK modulation it takes the values $\phi_m = m\frac{2\pi}{M}, 0 \leq m < M$. One important parameter of CSS modulations is the time-bandwidth product $B_{chirp}T_s$, also referred to as compression ratio or processing gain. Ideally $B_{chirp}T_s >> 1$ for observable gain in the symbols autocorrelation function at the output of the matched filter. In the system presented in Sec. V a binary modulation is used as initial analysis for simplicity and performance comparison with a traditional BPSK modulation. The two baseband up-chirp symbols of a CS-BPSK modulation, that is, from lower to higher frequency, are graphically represented in figure 3.

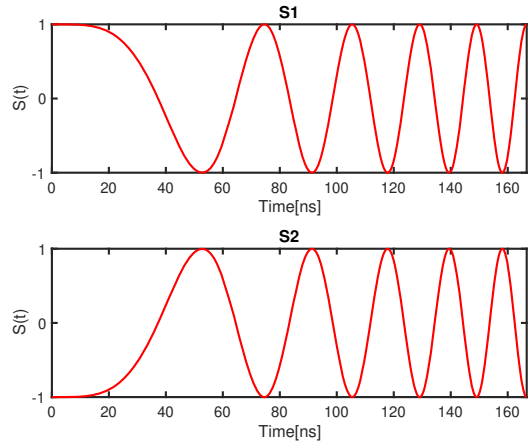

Fig. 3: Baseband symbols of the CS-BPSK modulation studied, with $B_{chirp} = 60$MHz and processing gain $BT = 10$

For CSS modulations, however, there exists a tradeoff between performance, in terms of error probability, and data rate. This tradeoff is reflected on the processing gain $B_{chirp}T_s$, and the symbol period T_s itself, which is directly related to the data rate. On the one hand, reduced T_s are desired for higher data rates but, on the other, the symbol energy over noise power spectral density ratio for a CSS modulation can be computed as:

$$\frac{E_s}{N_0} = SNR \ B_{chirp}T_s \tag{7}$$

From which falls that, for a fixed bandwidth and SNR, higher symbol periods are desired for a better performance of the modulation, that is, less probability of error. Therefore, the resiliency of CSS modulations in a given bandwidth comes at the expense of a lower data rate compared to traditional modulations using the same bandwidth. In the next section, we further explore this tradeoff by simulating a test case scenario where we report both the communications link budget and the radar performance that would be obtained from using the presented CS-BPSK modulation to jointly communicate and sense.

V. System Design and Problem Formulation

In this section we present the test-case scenario to study the proposed waveform and its main trade-offs. As highlighted in [16] and simulated in [17], space borne DAR platforms are better suited than ground-based DAR due to the high absorption in the lower troposphere. For this reason, we study the case in which a bi-static DAR is mounted as payload for a LEO satellite trying to transmit information to a ground station covered by clouds. Figure 4 depicts the scenario schematically. We focus on the case where the satellite transmits information to the ground stations, that is, the downlink. The sequence would go as follows: when the satellite comes up over the horizon from the ground station perspective, link budget conditions at low elevation angles might not be good enough for traditional modulations (QPSK, 8PSK, 16APSK, 32APSK) but, alternatively, good enough for CSS modulations. Therefore, transmission is initiated in JCS mode, where CSS modulation with the radar parameters for DAR are utilized. This allows the water vapor profile retrieval while transmitting information to the ground station. When a certain threshold elevation angle θ_{th} is reached by the satellite, link budget conditions might be good enough for traditional modulations. From that moment, the satellite could switch to those higher data rate modulations or stay in JCS mode if the satellite operator finds it adequate.

In order to asses the performance of both the communication link and the radar sensitivity we simulate the scenario for different values of elevation angle θ at the highest absorption frequency $f_3 = 174.8 \ GHz$. The dependence with the elevation angle comes from the fact that lower elevation angles mean larger slant paths through the atmosphere and, therefore, higher absorption losses. For the performance of the communications link we use the standard link budget equation from [26]:

$$SNR(\theta, f_3)_{gs} = P_{tx}G_{tx}\frac{1}{L(\ \theta, f_3)}\frac{G_{rx}}{T_0}\frac{1}{kBF_{gs}}, \tag{8}$$

where SNR_{gs} is the Signal to Noise Ratio at the ground station, P_{tx} is the transmitted power, G_{tx} and G_{rx} are the transmitter and receiver gains respectively, T_0 is the antenna temperature at the receiver, k is the Boltzman constant, B is

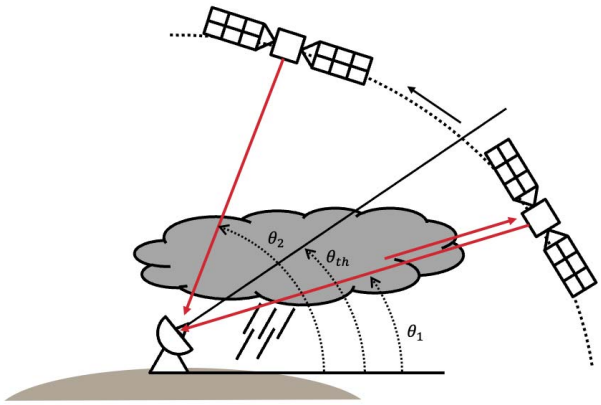

Fig. 4: Schematic of the scenario considered.

Satellite	
Parameter	Value
Altitude, h	200 km
Transmitted power, P_{tx}	200 mW
Transmitter gain, G_{tx}	48 dB
Bandwidth, B_{chirp}	60 MHz
Range resolution, Δr	2.5 m
Dielectric constant, $\|K\|^2$	0.93
Receiver noise temperature, T_0	290 K
Processing gain $B_{chirp}T_s$	10
Noise figure, F_{sat}	8 dB
Threshold SNR $SNR_{sat,th}$	1
Highest absorption transmit frequency f_3	174.8 GHZ

Ground station	
Parameter	Value
Receiver gain, G_{rx}	58 dB
Receiver noise temperature, T_0	290K
Receiver noise factor, F_{gs}	8dB

TABLE I: System parameters

the signal bandwidth, F_{gs} is the noise figure at the ground station receiver and L are the total path losses.

The total path losses considered for this link budget are characterized by spreading losses L_{spr} and molecular absorption losses L_{abs}. The absorption losses, related to molecular absorption, depend on the composition of the atmosphere, the temperature and the pressure. The two contributing losses are describes as

$$L_{spr}(f,d) = \left(\frac{4\ \pi df}{c}\right)^2, \text{ and} \tag{9}$$

$$L_{abs}(f,d) = \exp\left(\int_0^d k_a\left(f, Q(r), p(r), T(r)\right) dr\right) \tag{10}$$

where f stands for frequency, d stands for the total slant path length and k_a is the molecular absorption coefficient for the atmosphere, which depends on the composition Q, the pressure p and the temperature T. These parameters on their turn change across altitude. The values for the absorption losses are obtained from the ITU Recommendation ITU-R P.676-12 [27] as well as Recommendation ITU-R P.835 [28].

The figure of merit used to select a particular modulation and coding scheme in traditional satellite communication standards is the bit energy over noise power spectral density, or $\frac{E_b}{N_0}$. Therefore, in this analysis we compare the value of $\frac{E_b}{N_0}$ for a CS-BPSK modulation and for a traditional BPSK modulation given the same SNR. Although we compare binary modulations for simplicity and a direct relation between $\frac{E_b}{N_0}$ and the probability of error P_e, other higher order modulations could be used if the link quality is good enough. The relation between SNR and $\frac{E_b}{N_0}$ for a CS-BPSK is shown in (7), where $E_s = E_b$ in the case of binary modulations. On the other hand, this relation for BPSK is the following:

$$\frac{E_b}{N_0} = SNR_{gs}(1+\alpha), \tag{11}$$

where α is the roll-off factor of the square root raised cosine pulse utilized.

For the radar performance we study the minimum detectable reflectivity Z_{min} , or sensitivity, at the highest absorption frequency f_3 for different elevation angles and ranges. We utilize the standard weather radar equation from [24]:

$$Z_{min}(r,\theta,f_3) = \frac{1024\ln(2)\lambda^2}{\pi^5 P_{tx} G_{tx} \Delta r |K|^2} r^2 L_{abs}(r,\theta,f_3) \\ kT_0 B F_{sat}\ SNR_{sat,th}, \tag{12}$$

where r is the range at which the sensitivity is measured, λ is the wavelength at f_3, Δr is the radar range resolution, $|K|^2$ is the dielectric parameter, which for this analysis has been assumed to be constant at $|K|^2 = 0,93$. The factor kT_0BF_{sat} corresponds to the noise power at the satellite receiver and SNR_{sat} is the threshold SNR at which a reflected signal is discernible from noise. The absorption losses considered L_{abs} are computed with the same models as in the communications link budget. Table I reports the specific values used for the outlined parameters.

VI. Results

In this section we present the results obtained from simulating the scenario introduced in the previous section. As mentioned, we only compare binary modulations, but future work includes the extension of this analysis to higher order modulations. Figure 5 shows the link budget results of the simulated scenario, where the trade-off between data rate and time-bandwidth is observed. The vertical axis displays the different values of $\frac{E_b}{N_0}$ obtained from the SNR through (7) and (11) for the different elevation angles shown in the horizontal axis. A link quality threshold is added as a horizontal line at the $\frac{E_b}{N_0}$ value corresponding to an error probability $P_{error} = 10^{-6}$ for binary modulations. All the

curves displayed are computed with the same bandwidth, from Table I $B_{chirp} = 60\ MHz$, and a curve of a BPSK modulation using the same bandwidth and a roll-off factor $\alpha = 0.35$ is added for comparison.

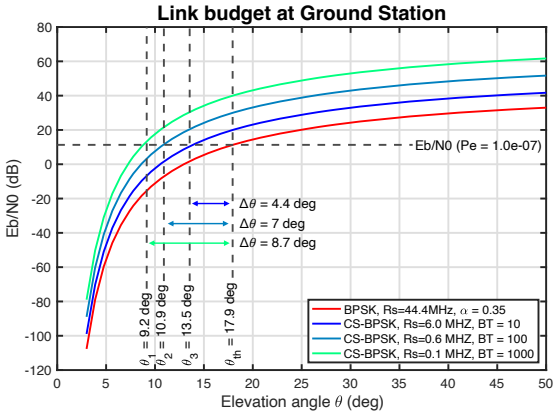

Fig. 5: Link budget performance for different elevation angles and time-bandwidth products. For low elevation angles, $\frac{E_b}{N_o}$ is not high enough for BPSK but high enough for CS-BPSK, making the transmission window larger as the time-bandwidth product increases

From the figure, we observe that higher time-bandwidth products result into better performance, reaching the $\frac{E_b}{N_0}$ threshold at lower elevation angles. This, combined with the satellite's orbital velocity, results into larger transmission windows, with the added benefit of sensing the in-cloud water vapor profiles above the ground station. However, for a fixed bandwidth, we observe that increasing the time-bandwidth product results into a decrease in symbol rate, i.e data rate in the binary case. Depending on the priority of the application, communication or radar, different values of time-bandwidth product should be considered. For example, if the priority is a high data rate, the satellite might choose to use CS-BPSK with low time-bandwidth product in the initial contact between the ground station and the satellite, but once the $\frac{E_b}{N_0}$ threshold for BPSK is reached, it would change to a traditional modulation with the corresponding data rate increase. On the other hand, if weather conditions above the ground station are harsh and data rate is not a priority, the satellite might be configured to vary the time bandwidth product from a high value to an intermediate one and use CS-BPSK during the whole transmission, providing a complete measurement of the water vapor conditions above the ground station.

In figure 6 we evaluate the sensitivity of the radar system as a function of distance from the satellite (range) and the elevation angle. Since the satellite is located at an altitude of $h = 200$ km, the range of distances evaluated covers the complete distance from the satellite to the Earth's surface. A semitransparent vertical plane is added at the limit of the atmosphere considered by the absorption models utilized $h = 100$ km. From (12), it can be inferred that the time-bandwidth product does not have a direct effect in the sensitivity of the system. However, chirp bandwidth and chirp time have separate indirect contributions that need to be taken into account when designing the satellite's sensing payload. On the one hand, larger values of B_{chirp} lead to more resolution, that is lower values of Δr. This however, leads to higher sensitivity of the system, which is not desired. On the other hand, larger values of chirp period T_s are desirable for larger integration times and therefore better SNR, but shorter values are desired for acquiring more time independent measurements and robustness against the decorrelation time corresponding to the aircraft-motion-induced Doppler spectrum. Therefore, there also exists a trade-off in the chirp parameters that needs to be further explored when designing the sensing parameters of the system.

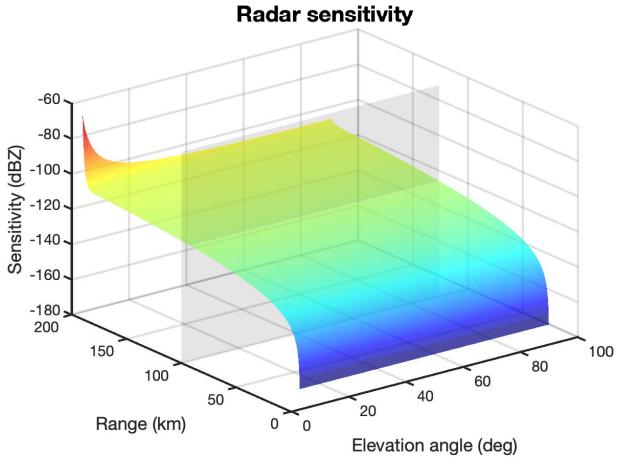

Fig. 6: Radar sensitivity, that is, minimum detectable signal, for a threshold $SNR_{sat,th} = 1dB$ at different ranges and elevation angles. A semitransparent vertical plane is added at the limit of the atmosphere considered by the absorption models utilized: $h = 100$ km

One important remark from Figure 6 is that the dependence with the elevation angle is only present in the lower layers of the atmosphere (Range $>$ 180 km), where the majority of absorption losses occur. This effect however could change depending of the weather situation above the ground station.

VII. Conclusions

In this paper, the Differential Absorption Radar technique, traditionally used for weather sensing, is explored as a potential candidate to be operated in combination with a Chirp Spread Spectrum (CSS) modulation for the joint transmission of information and remote sensing of the atmosphere. We present a scenario with a satellite at Low Earth Orbit (LEO) where the CSS modulation could outperform traditional PSK modulations while also make it possible to retrieve water vapor

density profiles of the atmosphere with DAR. Performance of both communication and remote sensing applications are studied through simulation, showing it is possible to develop a JCS system in the atmosphere and there exist scenarios where it even outperforms the use of traditional modulations. An important trade-off is found, however, when considering the chirp design parameters, particularly the chirp bandwidth B_{chirp}, the chirp period T_s and its product $B_{chirp}T_s$, known as the time-bandwidth product.Future lines of work include:

- Further study of the effect of the chirp design parameters on both the communications and sensing systems. For instance, fixing the symbol period and studying the required bandwidth to achieve the corresponding symbol rate is a promising approach to increase the data rate obtained with CSS modulations. This increase in bandwidth, however, should be compatible with the DAR requirements, if sensing capabilities are desired.
- Explore the use of higher order modulations. In the paper it is outlined that, if data rate is a priority, CS-BPSK modulation should be switched to traditional BPSK modulation when the link quality allows so. However, when link quality is good enough for BPSK, the corresponding $\frac{E_s}{N_0}$ for CS-BPSK is also much higher and higher order CS-MPSK modulations could be used to compensate the data rate difference.

ACKNOWLEDGMENT

The project that gave rise to these results received the support of a fellowship from "la Caixa" Foundation (ID 100010434). The fellowship code is LCF/BQ/AA20/11820041.

REFERENCES

[1] M. Giordani and M. Zorzi, "Satellite communication at millimeter waves: a key enabler of the 6g era," in *2020 International Conference on Computing, Networking and Communications (ICNC)*, Feb 2020, p. 383–388.

[2] J. Foust, "Spacex's space-internet woes: Despite technical glitches, the company plans to launch the first of nearly 12,000 satellites in 2019," *IEEE Spectrum*, vol. 56, no. 1, pp. 50–51, 2019.

[3] I. Mehdi, J. Siles, C. P. Chen, and J. M. Jornet, "Thz technology for space communications," in *2018 Asia-Pacific Microwave Conference (APMC)*. IEEE, 2018, pp. 76–78.

[4] P. Mróz, A. Otarola, T. A. Prince, R. Dekany, D. A. Duev, M. J. Graham, S. L. Groom, F. J. Masci, and M. S. Medford, "Impact of the spacex starlink satellites on the zwicky transient facility survey observations," *The Astrophysical Journal Letters*, vol. 924, no. 2, p. L30, 2022.

[5] P. H. Siegel, "Terahertz technology," *IEEE Transactions on microwave theory and techniques*, vol. 50, no. 3, pp. 910–928, 2002.

[6] P. Sen, V. Ariyarathna, A. Madanayake, and J. M. Jornet, "A versatile experimental testbed for ultrabroadband communication networks above 100 ghz," *Computer Networks*, vol. 193, p. 108092, Jul 2021.

[7] J. V. S. Perez, G. Chattopadhyay, C. Lee, E. T. Schlecht, C. D. Jung-Kubiak, and I. Mehdi, "On-chip power-combining for high-power schottky diode based frequency multipliers," Sep 2015. [Online]. Available: https://patents.google.com/patent/US9143084B2/en

[8] R. J. Roy, M. Lebsock, L. Millán, and K. B. Cooper, "Validation of a g-band differential absorption cloud radar for humidity remote sensing," *Journal of Atmospheric and Oceanic Technology*, vol. 37, no. 6, p. 1085–1102, Jun 2020.

[9] A. R. Nehrir, C. Kiemle, M. D. Lebsock, G. Kirchengast, S. A. Buehler, U. Löhnert, C.-L. Liu, P. C. Hargrave, M. Barrera-Verdejo, and D. M. Winker, "Emerging technologies and synergies for airborne and space-based measurements of water vapor profiles," *Surveys in Geophysics*, vol. 38, no. 6, p. 1445–1482, Nov 2017.

[10] J. V. Siles, K. B. Cooper, C. Lee, R. H. Lin, G. Chattopadhyay, and I. Mehdi, "A new generation of room-temperature frequency-multiplied sources with up to 10× higher output power in the 160-ghz–1.6-thz range," *IEEE Transactions on Terahertz Science and Technology*, vol. 8, no. 6, p. 596–604, Nov 2018.

[11] K. B. Cooper, "Imaging, doppler, and spectroscopic radars from 95 to 700 ghz," in *Passive and Active Millimeter-Wave Imaging XIX*, vol. 9830. SPIE, May 2016, p. 17–25.

[12] L. Millán, M. Lebsock, N. Livesey, and S. Tanelli, "Differential absorption radar techniques: water vapor retrievals," *Atmospheric Measurement Techniques*, vol. 9, no. 6, p. 2633–2646, Jun 2016.

[13] K. B. Cooper, R. Rodriguez Monje, L. Millán, M. Lebsock, S. Tanelli, J. V. Siles, C. Lee, and A. Brown, "Atmospheric humidity sounding using differential absorption radar near 183 ghz," *IEEE Geoscience and Remote Sensing Letters*, vol. 15, no. 2, p. 163–167, Feb 2018.

[14] R. J. Roy, M. Lebsock, L. Millán, R. Dengler, R. Rodriguez Monje, J. V. Siles, and K. B. Cooper, "Boundary-layer water vapor profiling using differential absorption radar," *Atmospheric Measurement Techniques*, vol. 11, no. 12, p. 6511–6523, Dec 2018.

[15] K. B. Cooper, R. J. Roy, R. Dengler, R. R. Monje, M. Alonso-Delpino, J. V. Siles, O. Yurduseven, C. Parashare, L. Millán, and M. Lebsock, "G-band radar for humidity and cloud remote sensing," *IEEE Transactions on Geoscience and Remote Sensing*, vol. 59, no. 2, p. 1106–1117, Feb 2021.

[16] R. J. Roy, K. B. Cooper, M. Lebsock, J. V. Siles, L. Millán, R. Dengler, R. R. Monje, S. L. Durden, F. Cannon, and A. Wilson, "First airborne measurements with a g-band differential absorption radar," *IEEE Transactions on Geoscience and Remote Sensing*, vol. 60, p. 1–15, 2022.

[17] R. J. Roy, M. Lebsock, and M. J. Kurowski, "Spaceborne differential absorption radar water vapor retrieval capabilities in tropical and subtropical boundary layer cloud regimes," *Atmospheric Measurement Techniques*, vol. 14, no. 10, p. 6443–6468, Oct 2021.

[18] T. Ince, "Fmcw radar performance for atmospheric measurements," vol. 19, no. 1, p. 7, 2010.

[19] A. Berni and W. Gregg, "On the utility of chirp modulation for digital signaling," *IEEE Transactions on Communications*, vol. 21, no. 6, p. 748–751, Jun 1973.

[20] A. Springer, W. Gugler, M. Huemer, L. Reindl, C. Ruppel, and R. Weigel, "Spread spectrum communications using chirp signals," in *IEEE/AFCEA EUROCOMM 2000. Information Systems for Enhanced Public Safety and Security (Cat. No.00EX405)*, May 2000, p. 166–170.

[21] B. Reynders and S. Pollin, "Chirp spread spectrum as a modulation technique for long range communication," in *2016 Symposium on Communications and Vehicular Technologies (SCVT)*, Nov 2016, p. 1–5.

[22] T. T. Nguyen, H. H. Nguyen, R. Barton, and P. Grossetete, "Efficient design of chirp spread spectrum modulation for low-power wide-area networks," *IEEE Internet of Things Journal*, vol. 6, no. 6, p. 9503–9515, Dec 2019.

[23] P. Sen, H. Pandey, and J. M. Jornet, "Ultra-broadband chirp spread spectrum communication in the terahertz band," *SPIE Defense + Commercial Sensing*, May 2020.

[24] M. I. Skolnik, *Introduction to radar systems*, 2nd ed. McGraw-Hill, 1980.

[25] "Manual of regulations and procedures for federal radio frequency management (redbook) national telecommunications and information administration," https://www.ntia.doc.gov/page/2011/manual-regulations-and-procedures-federal-radio-frequency-management-redbook.

[26] G. Maral and M. Bousquet, *Satellite communications systems: systems, techniques and technology*, 5th ed. John Wiley and Sons, 2009.

[27] "Attenuation by atmospheric gases and related effects," *International Telecommunication Union*, vol. P.676-12, 2019.

[28] "Reference standard atmospheres," *International Telecommunication Union*, vol. P.835-6, 2017.